Annealing Study of Dilute Aluminum Alloys Electron Irradiated at Liquid-Nitrogen Temperature*

M. Doyama[†]

Argonne National Laboratory, Argonne, Illinois 60439

and

J. S. Koehler

Materials Research Laboratory and the Department of Physics, University of Illinois, Urbana, Illinois

and

Y. N. Lwin,[‡] E. A. Ryan, and D. G. Shaw[§]

Argonne National Laboratory, Argonne, Illinois 60439

Pure and dilute aluminum alloys (Mg, Zn, Ag, Ge, Au, and In) were irradiated at about 90 °K by 2- or 3-MeV electrons. Isothermal annealing for 30 min at temperature intervals 10 °C apart was carried out. The major results were the following: Stage-III annealing occurs by a second-order process with an activation energy $E_{III} = 0.60 \pm 0.04$ eV for both pure and dilute aluminum alloys. Since this activation energy is the same as that found by quenching experiments, it is concluded that stage III in aluminum and dilute aluminum alloys occurs by the motion of vacancies. Two stages below stage III are dependent on the kind of impurity. A mechanism consisting of a breakup of interstituals from impurity traps (single-impurity atoms or impurity-atom clusters) can explain the experimental results. Reverse recovery of electrical resistivity was observed below and above stage III; this is due to Guinier-Preston-zone formation.

I. INTRODUCTION

The low-energy electron irradiation of metals at low temperature is likely to produce a particularly simple distribution of point defects in metals. Annealing of irradiated metals shows only a few recovery stages. They have been called stage I (below 60 °K), stage II (60 °K < T < 220 °K), stage III (220 °K < T < 450 °K), and stage IV.

The stage-I recovery is generally ascribed to the annihilation of close pairs (interstitial vacancy) and the long-range migration of an interstitial-defect species.[1] One of the important processes in stage II is associated with the recovery of interstitials released from impurity traps, shallow ones at lower temperatures and deeper ones at higher temperatures.[2,3] There is relatively little experimental data concerning stage IV.

The recovery of electrical resistivity in pure Al and Al alloys following neutron and electron irradiation at various temperatures has been one of the most studied approaches. Table I summarizes the results of some previous investigations of both pure and alloyed aluminum. The purpose of the present research is to study the effects of impurities on stage-III annealing and the recovery between liquid-nitrogen temperature (the temperature of irradiation) and stage III.

II. EXPERIMENTAL PROCEDURES

A. Specimen Preparation and Mounting

The alloy specimens used were supplied in the form of 40-mil-diam wire (nominally 99.9999% aluminum and dopants) by Cominco. These wires were drawn to a diameter of 5 mil. The wires were etched with a hot mixture of 95% phosphoric acid and 5% nitric acid between drawings. The specimens were mounted in the manner described by Dworschak, Herschbach, and Koehler.[17] For those specimens annealed at temperatures higher than 60 °C, thin-cleaved mica sheets were used in place of Mylar sheets used in previous experiments.[8]

The annealing of alloy specimens was carried out in air. The furnace used for annealing was suddenly heated and shut off when it reached 450 °C. The specimens were allowed to cool to room temperature in the furnace. The annealing of some of the alloy specimens was carried out in a vacuum furnace. The results were found to be the same as those in air.

B. Irradiation Procedure

The liquid-nitrogen cryostat used is described by Lwin, Doyama, and Koehler.[8] The Van de Graaff machine of the Materials Research Laboratory at the University of Illinois was used for the present experiments. The cryostat was visually aligned with respect to the electron beam. The beam uniformity was checked by irradiating a glass slide mounted on a dummy block with a short pulse (a few seconds) of electrons. The uniformity in color, due to formation of color centers in the glass slide, gave a good indication of the uniformity of

TABLE I. Summary of experimental results for stage III in pure and dilute alloys of aluminum.

References	Material	Irradiation	Model supported or proposed	Activation energy
4–7	Pure Al 0.1% Cu, Mn, Si Zn, Ag, Sn, Mg	Neutron ~78 °K	Vacancy	0.6 ± 0.04
8	Pure Al	Electron ~90 °K	Vacancy	0.61 ± 0.04
9	Pure Al 0.1% Zn	Electrons ~4.2 and ~78 °K	Interstitial	0.45 ± 0.01
10	Pure Al 0.1% Mg, Ga, Ag	Electron ~10 °K	Interstitial	Pure ~0.53 Alloys 0.62
11	Pure Al 0.3% Zn, Cu, Ge	Electron 10–80 °K	Vacancy	• ° °
12	Pure Al Quenched Al	Electron ~10 °K	Interstitial	0.58
13–15	Pure Al wide range of Mg alloys	Neutron ~78 °K	° ° °	
16	Pure Al	Electron ~100 °K	Interstitial	0.55 ± 0.03

the beam. To monitor the temperature rise during irradiation and later during recovery, a copper-constantan thermocouple (2 mil diam) was attached to a dummy specimen mounted in each block. The energy of the electron beam was regulated to within 0.025 MeV at 2 or 3 MeV.

After passing through three windows of 1-mil Al foil, the incident beam of electrons was estimated to have an energy of 1.94 MeV (for 2-MeV initial energy). At this energy, the range is approximately 140 mil, sufficient to insure a homogeneous distribution of defects in 5-mil-diam samples.

The beam current was limited to 7.5 μA/cm^2, which resulted in a sample temperature of no higher
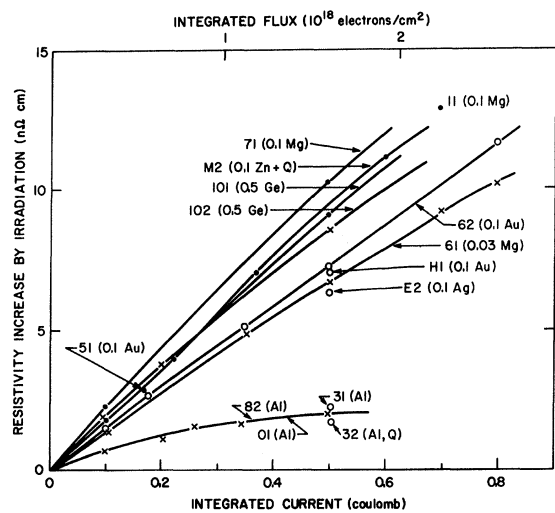

FIG. 1. Resistivity increase as a function of integrated electron flux for samples bombarded by 3-MeV electrons at 80 °K.

than 100 °K. For the dummy sample, the decrease in thermal conductivity for increasing defect concentration resulting from the irradiation was observed from the steady gradual rise in temperature throughout each irradiation.

In order to investigate the production damage by electron irradiation, some samples were removed from the beam, measured at 4.2 °K, and returned for further irradiation. With this procedure, production curves for eight different samples were obtained (Fig. 1).

C. Resistivity Measurement and Annealing

The resistance of all samples was measured at liquid-helium temperature by immersion of the sample block in this liquid. The method was a standard potentiometric method. The current was supplied by a constant-current supply (Fluke Model 318). The voltage across the specimen was measured by a Rubicon six-dial thermofree microvolt potentiometer in conjunction with a Rubicon photoelectric galvanometer. The effect of stray thermal emf's in the circuit was eliminated by reversing the current direction and taking the average of the readings for the two current directions.

Sample blocks were annealed in an immersion bath. This consisted of a double-Dewar system with liquid nitrogen as a cooling source and an electric heater for heating. The deviations between the platinum resistance thermometer used to measure the bath temperature and the set point, the desired annealing temperature, were approximately 0.2 μV, corresponding to a temperature variation of less than ±0.025 °C.

In order to extend the operating range of the annealing bath, liquid Freon No. 12 (CF$_2$Cl$_2$) was used up to – 40 °C, alcohol was used for – 40 °C $\leq T \leq$ 50 °C,

TABLE II. Summary of data for irradiated samples.

Specimen block	Material and type	Fig.	Resistivity before irradiation $(10^{-9} \ \Omega cm)$	Resistivity after irradiation $(10^{-9} \ \Omega cm)$	Radiation induced resistivity $(10^{-9} \ \Omega cm)$	Total electron fluence $(10^{18} el/cm^2)$	Treatment given
L D2	Al + 0.08% Mg		37.48	47.67	10.19	3.1	Isothermal (29 °C) (4, 4, 8, 16, 32 min)
L A2	Al + 0.08% Mg		37.97	42.54	4.57	1.56	Isothermal (20 °C) (4, 4, 8, 16, 32 min)
L G2	Al + 0.09% Mg		° ° °	40.40	° ° °	1.56	Isochronal (30 min) 10 °C
L J1	Al + 0.08% Mg		° ° °	38.41	° ° °	1.56	Isochronal (10 min) 10 °C
L 01	Al + 0.08% Mg		° ° °	38.38	° ° °	1.56	Isochronal (30 min) 10 °C
L A1	Al + 0.1% Ag		115.58	120.82	5.24	1.56	Isothermal (20 °C) (4, 4, 8, 16, 32 min)
L J2	Al + 0.1% Ag	10	° ° °	117.94	° ° °	1.56	Isochronal (10 min) 10 °C
L 02	Al + 0.1% Ag		° ° °	116.52	° ° °	1.56	Isochronal (30 min) 10 °C
L 52	Al + 0.003% Au	7	2.56	4.92	2.36	1.56	Isochronal (10 min) 10 °C
L G1	Al + 0.003% Au		° ° °	2.58	° ° °	1.56	Isochronal (30 min) 10 °C
L 21	Al + 0.003% In		2.96	4.60	1.64	1.56	Isochronal (30 min) 10 °C
L F2	Al + 0.003% In		° ° °	2.99	° ° °	1.56	Isochronal (10 min) 10 °C
L F1	Al + 0.1% Zn		° ° °	2.28	° ° °	1.56	Isochronal (10 min) 10 °C
B1	Al + 0.1% Mg	4, 8	34.57	40.33	5.76	0.94	Isothermal (10 °C) (4, 4, 8, 14 min)
B2	Al + 1.5% Mg		° ° °	550.02	° ° °	0.94	Isothermal (10 °C) (4, 4, 8, 14 min)
21	Al + 0.1% Mg	2, 4, 8	35.83	44.97	9.14	2.18	Isothermal (10 °C) (4, 4, 8, 14 min)
22	Al + 1.5% Mg	4, 8	565.07	580.04	14.97	2.18	Isothermal (10 °C) (4, 4, 8, 14 min)
61	Al + 0.03% Mg	4, 8	9.43	19.61	10.18	2.5	Isothermal (10 °C) (4, 4, 8, 14 min)
11	Al + 0.1% Mg	4, 8	35.43	48.27	12.84	2.2	Isothermal (10 °C) (4, 6, 8, 12 min)
12	Al + 1.5% Mg	4, 8	563.40	579.53	16.13	2.2	Isothermal (10 °C) (4, 6, 8, 12 min)
71	Al + 0.1% Mg		35.99	46.11	10.12	1.56	Isothermal (at −150 °C, −85 °C, −55 °C)
M1	Al + 0.1% Zn	5, 9	22.47	33.51	11.04	1.88	Isothermal (10 °C) (4, 6, 8, 12 min)
M2	Al + 0.1% Zn	5, 9	34.12	45.85	11.73	1.88	Specimen prequenched Isothermal (10 °C) (4, 6, 8, 12 min)
A1	Al + 0.1% Zn	5, 9	° ° °	29.52	° ° °	1.56	Specimen prequenched Isothermal (10 °C) (4, 6, 8, 12 min)
A2	Al + 0.1% Zn	3, 5, 9	° ° °	28.76	° ° °	1.56	Isothermal (10 °C) (4, 6, 8, 12 min)
E1	Al + 0.03% Ag	10	33.36	39.23	5.87	1.56	Isothermal (10 °C) (4, 6, 8, 12 min)
E2	Al + 0.1% Ag	10	111.19	117.34	6.15	1.56	Isothermal (10 °C) (4, 6, 8, 12 min)
101	Al + 0.5% Ge	6	338.13	347.26	9.13	1.56	Isothermal (10 °C) (4, 4, 8, 14 min)

TABLE II. (*continued*)

Specimen block	Material and type	Fig.	Resistivity before irradiation (10^{-9} Ωcm)	Resistivity after irradiation (10^{-9} Ωcm)	Radiation induced resistivity (10^{-9} Ωcm)	Total electron fluence (10^{18} el/cm^2)	Treatment given
102	Al +0.1% Ge	6	78.99	87.50	8.51	1.56	Isothermal (10 ?C) (4, 4, 8, 14 min)
R1	Al +0.5% Ge	6	333.76	345.67	11.91	1.56	Isothermal (10 °C) (4, 6, 8, 12 min)
R2	Al +0.1% Ge	6	78.84	87.58	8.74	1.56	Isothermal (10 °C) (4, 6, 8, 12 min)
62	Al +0.1% Au	11, 16	36.65	48.29	11.64	2.5	Isothermal (10 °C) (4, 4, 8, 14 min)
51	Al +0.1% Au	7, 11, 16	33.67	36.54	2.87	0.544	Isothermal (10 °C) (4, 4, 8, 14 min)
D1	Al +0.1% Au		34,10	44.41	10.31	2.03	Isochronal (10 min) 10 °C
H1	Al +0.1% Au		33.88	40.83	6.95	1.56	Isothermal (at −150 °C, −85 °C, −55 °C, −15 °C) Kinetics

water was used 50 °C $\leq T \leq$ 90 °C, and oil was used above 100 °C. Liquid freon No. 12 has a larger operating range and fewer hazards than those used previously.[8] The lowest operating temperature obtained with this liquid was − 155 °C. The difference in temperature between the dummy specimen and the bath was measured with a thermocouple attached to the dummy, the reference temperature being that of the bath. These readings were recorded throughout the anneal and corrections similar to those described by Grenning and Koehler[18] for the warmup time were calculated using a CDC 3600 computer at Argonne National Laboratory.

FIG. 2. Isothermal recovery of the electrical resistivity increase $\Delta\rho$ between − 150 and 100 °C for specimen 21 (Al +0.1 at. % Mg) following electron irradiation near 80 °K.

III. EXPERIMENTAL RESULTS

A total of 35 specimens, mounted on 20 different specimen blocks, were irradiated with 2- and 3-MeV electrons near liquid-nitrogen temperature in 20 different irradiation runs. Specimen names labeled $L(L$ specimens) were irradiated with 2-MeV electrons; the others were irradiated with 3-MeV electrons. Table II gives the composition of the specimens, the integrated flux used, the radiation-induced resistivity, and treatment after irradiation.

A. Damage Production

The resistivity increase by irradiation is plotted against electron fluence for Al and Al alloys. From Fig. 1, the resistivity increase due to irradiation is largest for those samples which have the highest concentration of dopants and smallest for pure aluminum doped with vacancies. The plot of the logarithm of damage vs the logarithm of the electron flux for pure aluminum shows a definite concave-downward curvature. For dilute-alloy specimens, the production curve is nearly linear, but again shows the concave feature. Although the simple relation $\Delta\rho = A\varphi^n$ does not give a perfect fit, n was found to be 0.6 for pure aluminum, 0.75 for less-pure aluminum, and about 0.9 for dilute alloys. For the same concentration 0.1 at.% the production rate as measured by electrical resistivity decreases as the atomic mass of the dopant increases (Mg, Zn, Ge, Ag). This result is not unreasonable if one considers energy-transfer mechanisms such as direct displacement of impurity
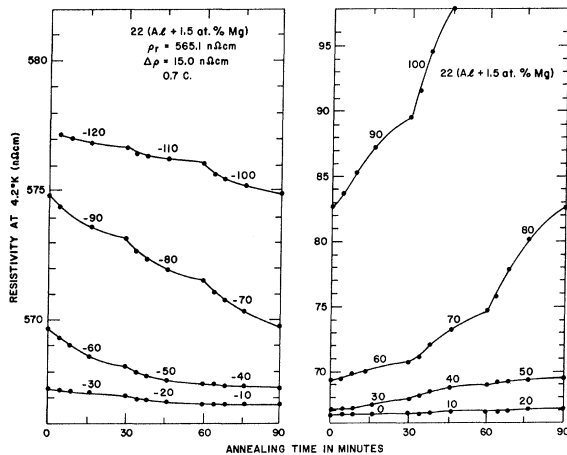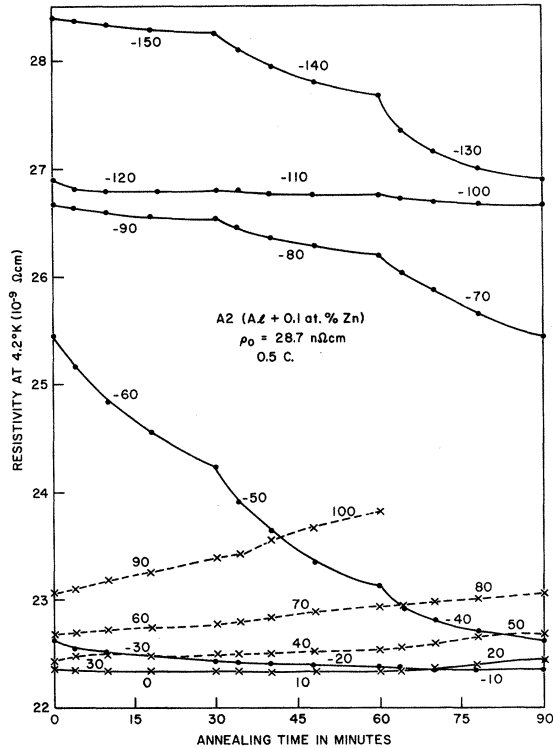
FIG. 3. Isothermal recovery of the electrical resistivity increase $\Delta\rho$ between -150 and $100\,°C$ for specimens A2 (Al $+0.1$ at. % Zn) following 3-MeV electron irradiation near 80 °K.
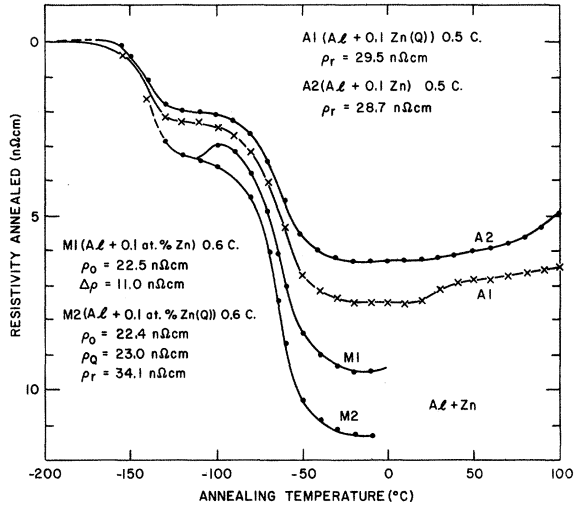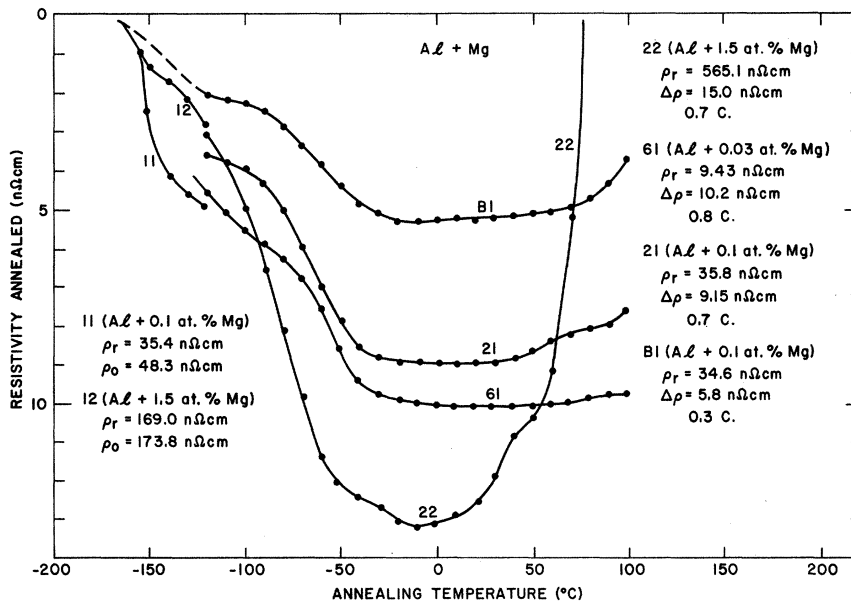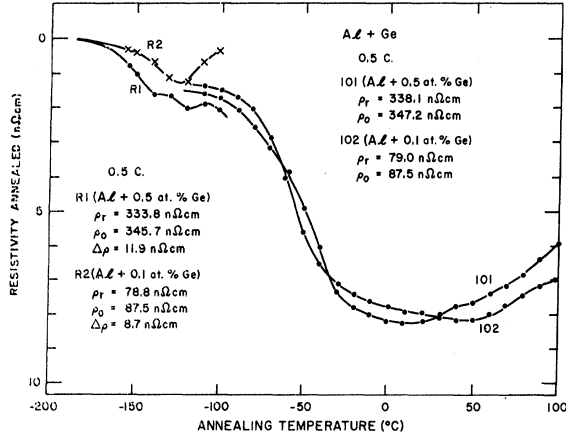

FIG. 5. Isochronal recovery of the electrical resistivity increase $\Delta\rho$ for Al specimens containing Zn following electron irradiation near 80 °K, and annealed for 30 min every 10 C°.

atoms. Furthermore, it has been brought to the authors' attention that the capture cross section of the impurity could play an important role in deter-

mining the production rate. Alloys doped with Au however do not follow this scheme. The total integrated fluxes were between 3×10^{17} and 2.5×10^{18} electrons/cm^2.

B. Isothermal-Isochronal Annealing

Isothermal annealing was carried out at temperatures successively 10 °C apart from $-150\,°C$ to $100\,°C$. 20 specimens of Al and Al alloys were given this treatment. At each temperature, the residual resistivity remaining, as measured at li-

FIG. 4. Isochronal recovery of the electrical resistivity increase $\Delta\rho$ for Al specimens containing Mg following electron irradiation near 80 °K, and annealed for 30 min every 10 C°.

FIG. 6. Isochronal recovery of the electrical resistivity increase $\Delta\rho$ for Al specimens containing Ge following electron irradiation near 80 °K, and annealed for 30 min every 10 C°.

quid-helium temperature, was determined after 4, 10, 18, and 30 min of total annealing time. Other specimens (L specimens) were annealed at temperatures successively 20 °C apart from − 120 °C to 75 °C and measured after 4, 8, 16, 32, and 64 min. The temperature rise in the dummy specimen was recorded in each case and annealing times were corrected. This correction can be eliminated by choosing the starting time of the anneal appropriately.

The results consisting of segments of isothermal anneals for two of the specimens are shown in Figs. 2 and 3. From all of the isothermal curves, isochronal curves were constructed. A few representative curves are shown in Fig. 4–7. The total annealing times are 30 min at each temperature. The experimental points are connected with a "smooth" curve. Each smooth segment between two experimental points was obtained from a seventh-order polynomial fitted to eight neighboring points. The procedure was then shifted to the next data point producing the "smooth" curve. The corresponding slopes of the isochronal curves were obtained by differentiating these seventh-order polynomials and connecting these slopes to produce, for example, Figs. 8–12. A CDC 3600 digital computer at Argonne National Laboratory was used for these calculations. Recently there has been some discussions regarding the methods of calculating activation energies.[12] We chose here the change-of-slope method.[19] The isothermal intervals were changed compared to a previous experiment[8] in order to obtain more accurate values.

In the isochronal anneals for pure aluminum, the main peak (so-called stage III) was found near − 40 °C with two small peaks A at − 120 °C and B at − 150 °C (Fig. 12). These two small peaks grow

as the impurity content increases. The main peak shifts to lower temperatures as the dose increases.[8] The activation energy of this peak was found to be 0.60 ± 0.03 eV.

Aluminum-zinc alloys show enhanced A peaks and a main peak C shifted to − 60 °C, appreciably lower than that for pure aluminum (Fig. 9); the half-width of the main peak is about 30 C°, which is approximately the same as for pure aluminum. The activation energy for this stage was calculated to be 0.60 ± 0.03 eV. The temperature of A peak was found to be almost constant at − 137 °C for 30-min isochronal anneals. Slight shifts of this peak were attributed to differences in dose; for larger doses, a slight increase in the annealing-peak temperature was observed. The activation energy associated with this peak was approximately 0.37 ± 0.02 eV. The small shoulder (peak B) was not enhanced as much as peak A. Since the main C peak was shifted to a lower temperature, the clear separation seen in pure aluminum is greatly reduced.

If the breakup process in which interstitials break away from a zinc atom or small zinc cluster is occurring in this stage, then the binding energy for this process would be $0.26 = 0.37 − 0.11$ eV. Guinier-Preston-zone (GP-zone) formation was observed above 20 °C (see Fig. 3). A small reverse recovery was observed below stage III (sample $M1$, Fig. 5), which may be due to the motion of a vacancy-impurity complex forming GP zones before
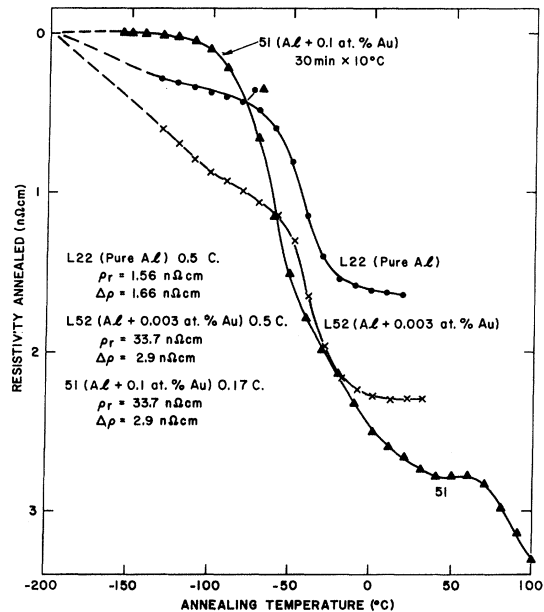

FIG. 7. Isochronal recovery of the electrical resistivity increase $\Delta\rho$ for Al specimens containing Au following electron irradiation near 80 °K, and annealed for 30 min every 10 C°.
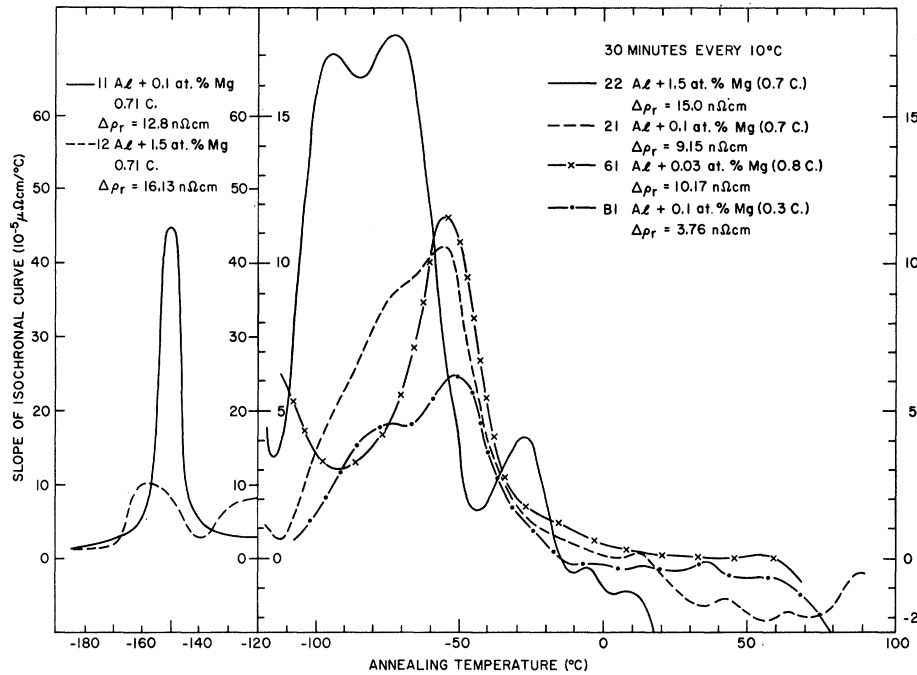
FIG. 8. Slope os isochronal recovery curve for specimens containing Mg irradiated with electrons near 80 °K and annealed for 30 min every 10 C°.

the actual stage III begins. These vacancy-impurity pairs could be formed by knocking out an aluminum atom next to a zinc atom by electron irradiation. This could happen because the core size of a zinc atom is fairly large compared with that of an aluminum atom giving larger displacement probability to an aluminum atom which is a nearest neighbor to the zinc impurity. Federighi[20] has stated that based on recovery measurements of

quenched Al-Zn alloys, a Zn-impurity atom seems to migrate with a lower activation energy than single vacancies. This, along with the low binding energy between a zinc impurity and vacancy, leads us to suggest that it is possible that the vacancy-zinc complex can also move more easily than an isolated vacancy.

Al-Mg alloys have distinct peaks in our isochronal-annealing curves. One peak is near −150
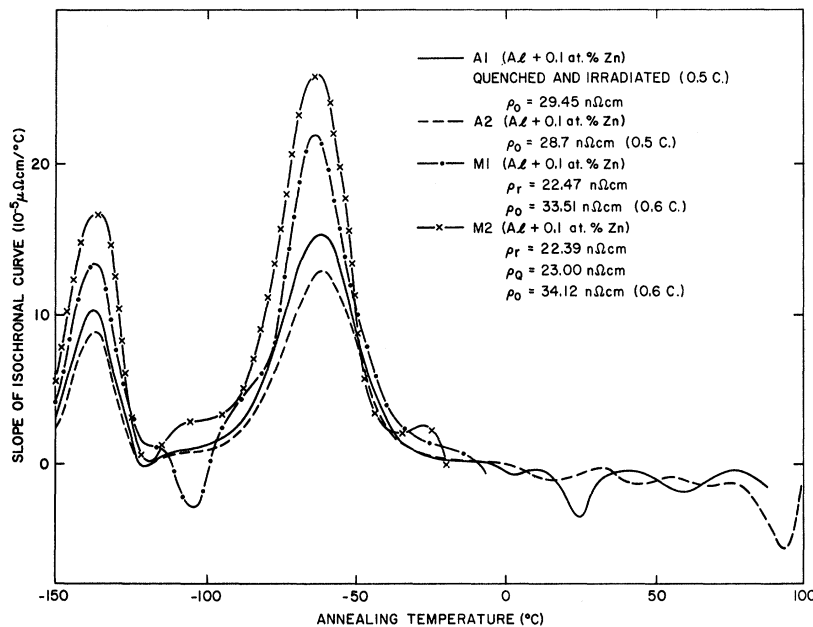

FIG. 9. Slope of isochronal recovery curve for specimens containing Zn irradiated with electrons near 80 °K and annealed for 30 min every 10 C°. Specimens A1 and M2 were quenched before irradiation.
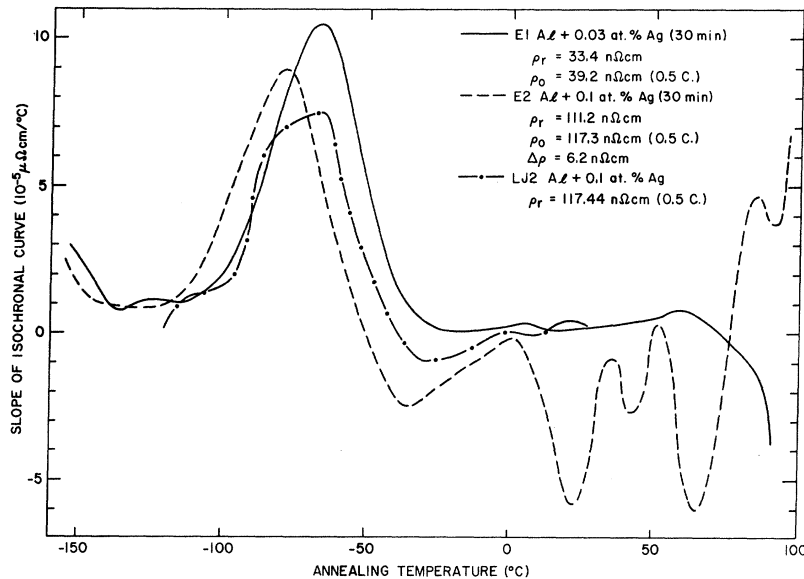
FIG. 10. Slope of isochronal recovery curve for specimens containing Ag irradiated with electrons near 80 °K and annealed for 30 and 10 min every 10 C°.

°C. The other two fuse together to form a doublet whose midtemperature is dose dependent. The -150 °C peak of Al–1.5 at.% Mg is not as sharp as that of Al–0.1 at.% Mg. The activation energy associated with this peak is 0.30 ± 0.04 eV. The lower peak of the doublet B peak is greatly enhanced compared with that of pure aluminum (Fig. 8). For samples containing the same concentration of magnesium the midpoint of the B peak is shifted to higher temperatures with increased dose: Compare $B1$ and 21 (Fig. 8). The activation energy for the B peak is 0.54 ± 0.04 eV, and that for C peak is (0.61 ± 0.04) eV. Again GP-zone formation is clearly seen in Al-Mg alloys, particularly in those

specimens with higher magnesium concentrations, i. e., sample 22 in Fig. 4. Garr and Sosin[10] irradiated Al-Mg alloys and observed one stage near 80 °K and another at 130 °K. Their 130 °K peak is the same process we observed at -137 °C. If this stage results from the breakaway of interstitials from a magnesium atom or small magnesium clusters, it follows that the binding energy between an interstitial and magnesium impurity is about $0.37 - 0.11 = 0.26$ eV. For the same dose the stage on the lower side of the doublet grows as the impurity concentration is increased (Fig. 8). For Al-0.03-at.%-Mg alloy, sample 61, this peak was not recognizable (Fig. 8). This could be due to the release
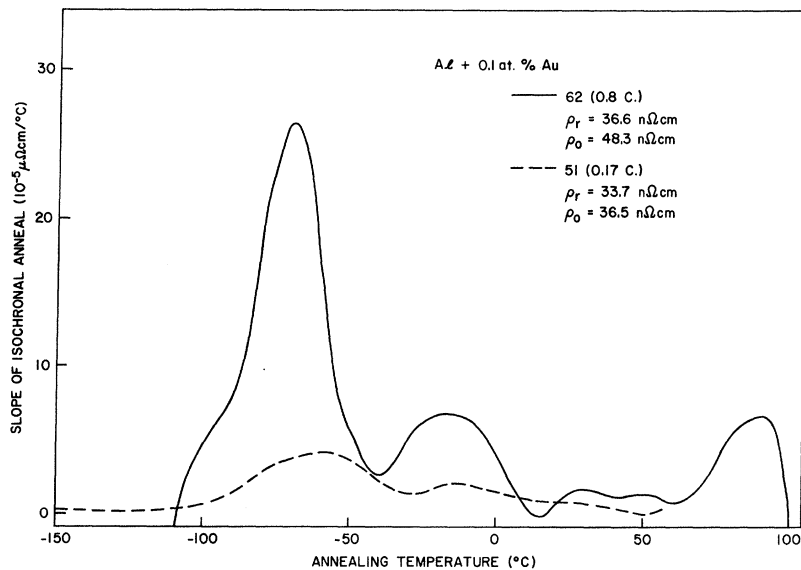

FIG. 11. Slope of isochronal recovery curve for specimens containing Au irradiated with electrons near 80 °K and annealed for 30 min every 10 C°.
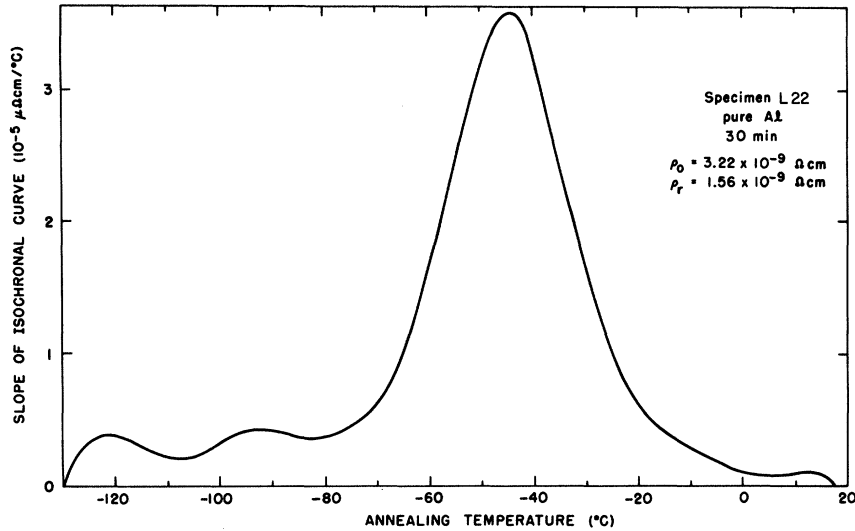
FIG. 12. Slope of isochronal recovery curve for pure-Al specimens irradiated with 2-MeV electrons near 80 °K and annealed for 30 min.

of interstitials from dimagnesium agglomerates. The binding energy between an interstitial and the defect is $0.43 = 0.54 - 0.11$ eV.

Al-Ag alloys again show essentially the same three-peak structure seen in Al-Mg alloys. The peak around -150 °C is distinct and its activation energy is 0.35 ± 0.03 eV. The other peaks B and C fuse together (Fig. 10). The width of the fused peak is about 37 °C, which is wider than that of pure aluminum. This is an indication of two overlapping peaks. The activation energy associated with the low-temperature side of the peak is 0.55 ± 0.33 eV, and that of the main peak is again 0.61 ± 0.03 eV. For the Al-0.1-at.%-Ag alloy, sample $E2$, the GP-zone formation is seen above -50 °C with the maximum resistivity at 80 °C. For these alloys, the binding energy between an interstitial and a defect would be $0.24 = 0.35 - 0.11$ eV if the breakup process occurs.

The results for Al-Au alloys differ from the other alloys mentioned above. When the gold content is high, suppression of the low-temperature peak (at $\simeq -140$ °C) is complete. The main peak has a small shoulder (peak B) and shifts with dose (Fig. 11). The activation energy for the main peak is 0.61 ± 0.03 eV. A new peak can be seen near -15 °C and its midtemperature shifts to lower temperatures as the dose increases. The activation energy for this peak is 0.69 ± 0.03 eV. The peak near 90 °C has an activation energy of 1.02 ± 0.05 eV. The reverse recovery due to GP-zone formation was not seen in gold alloys. Al-Au alloys do not have any distinct stages below stage III (Fig. 11). The solubility of gold in aluminum is very small. [21] It is likely that most of the gold atoms in 0.1-at.%-Au alloys are not dissolved but are precipitated. Interstitials may be trapped at these small precipitates quite strongly as well as at iso-

lated gold atoms in this alloy.

Al-Ge alloys have three peaks, one at -140 °C and a large peak at about 55 °C with a definite shoulder. The activation energy associated with the peak at -140 °C is 0.34 ± 0.03 eV, that of the low-temperature shoulder 0.47 ± 0.04 eV, and that of the main peak 0.61 ± 0.03 eV. The peak in Al-0.1 at.% Ge (Sample 102) is quite broad ($\simeq 44$ °C). The GP-zone formation is apparent above 30 °C. An increase in resistivity below -100 °C for this alloy was observed. This again is possibly due to
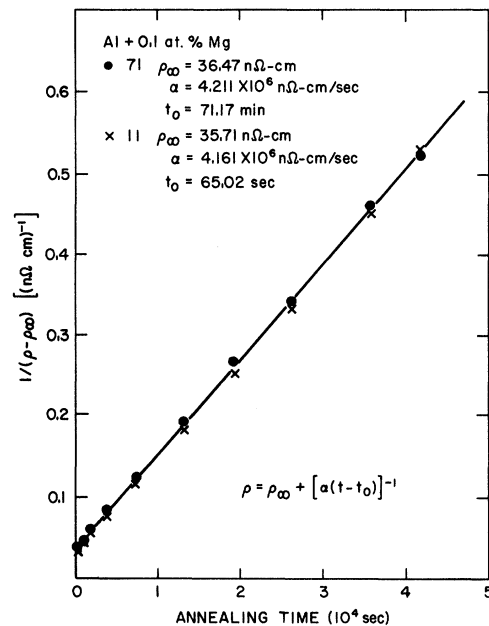

FIG. 13. Long isothermal annealing of electron irradiated Al-0.1-at.%-Mg alloy. Two specimens were isothermally annealed at -55 °C for 850 min.
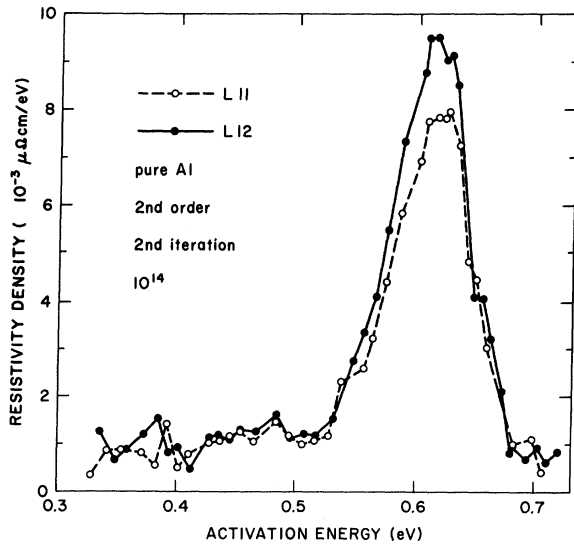
FIG. 14. Activation-energy spectrum for pure Al.

the GP-zone formation.

The results for In-doped alloys are similar to those for pure aluminum because of the low dopant concentration.

C. Determination of Order of Kinetics

The rate of resistivity change is often written as

$$-\frac{d(\Delta\rho)}{dt} = \Gamma\,(\Delta\rho)^n e^{-E/kT} , \tag{1}$$

where $\Delta\rho$ is the resistivity remaining after annealing, E is the activation energy of annealing, T is the absolute temperature of annealing, k is Boltzmann's constant, t is annealing time, Γ is a constant, and n is the order of kinetics. $\Delta\rho$ can be written in the form of $\Delta\rho = \rho - \rho_\infty$, where ρ is the resistivity at time t and ρ_∞ is the resistivity after complete annealing of the process. For $n = 2$, the solution of Eq. (1) becomes

$$\frac{1}{\rho - \rho_\infty} - \frac{1}{\rho_0 - \rho_\infty} = \Gamma\,(t - t_0)e^{-E/kT} . \tag{2}$$

Here ρ_0 is the resistivity at $t = 0$. A disadvantage associated with the use of Eq. (2) is the need to extrapolate the annealing process to completion. Various attempts have been made to circumvent this problem but these methods also have certain difficulties.[22,23] In this paper, the equation

$$\rho = \rho_\infty + [\alpha(t - t_0)]^{-1} \tag{3}$$

was used. ρ_∞, α, and t_0 were obtained by the least-squares method using the CDC 3600 digital computer at Argonne National Laboratory. Figure 13 is one of the typical curves.

D. Determination of Activation-Energy Spectrum

The annealing of kinetic processes with a distri-

bution of activation energies has been discussed in detail by Primak.[24] The calculation of activation-energy spectra for first-order process has been carried out by Magnuson, Palmer, and Koehler,[25] by Bredt,[26] by Herschbach,[27] and by Bauer, DeFord, Koehler, and Kauffman.[28] This method has been applied to second-order processes by Dworschak, Herschbach, and Koehler.[17]

In this work the activation-energy spectra were determined under the following assumptions: (a) independent processes are distributed in activation energy, and (b) the frequency factor is constant.

The values of the constants necessary for these calculations have been determined such that the best smooth curve can be obtained. Figures 14–16 show the activation-energy spectra for pure aluminum, aluminum-zinc, and aluminum-gold alloys, respectively. The uncertainty of the values of the constants introduces an error in determining the activation energy of about 0.03 eV. The integrals were evaluated using Gauss's mechanical quadrature formula,[29] order 16, and the CDC 3600 digital computer.

The activation-energy spectra for Al alloys are analyzed by a method detailed above. The spectra have essentially the same features as the corresponding differential isochronal annealing curves. (Compare Figs. 12 and 14, 9 and 15, 11 and 16.) Table III gives the results obtained for some of the sam-
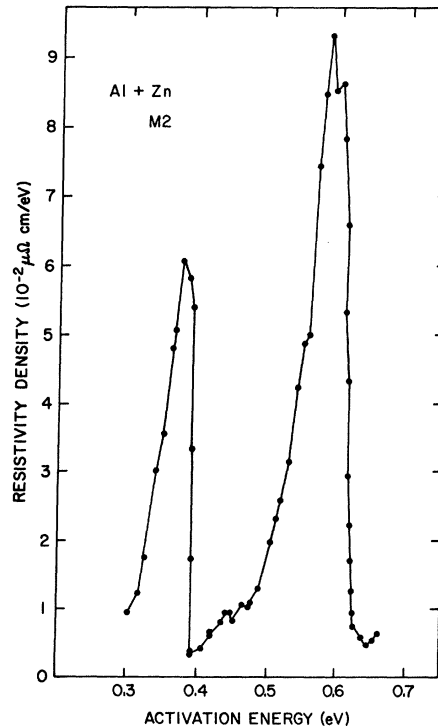

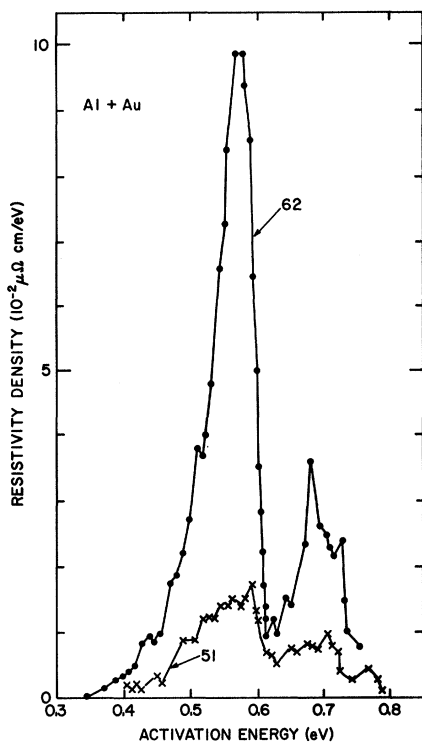FIG. 15. Activation-energy spectrum for Al-Zn alloys.

FIG. 16. Activation-energy spectrum for Al–Au alloys.

ples.

IV. SUMMARY AND CONCLUSIONS

There are several surprising facts which the present experiments reveal concerning stage-III annealing of electron-irradiated alloys. They are the following:

(a) In all of these dilute alloys an annealing peak that occurs after electron irradiation has an activation energy of 0.60 eV, which is just the vacancy-migration energy seen in pure aluminum after quenching from low temperature. This indicates that for many of the vacancies, migration to the interstitial-impurity clusters occurs with fewer atomic jumps than migration to an isolated impurity or an impurity cluster. It is possible that the impurities are not present as single-impurity

atoms but consist of small impurity clusters. Furthermore, it is conceivable that the activation energy for the motion of impurity-vacancy complex studied in this research is the same or lower than that for single vacancies. Peterson and Rothman[30] find that Ge, Ga, Zn, Ag, and Au diffuse into aluminum with almost the same activation energy as the activation energy of the self-diffusion in aluminum.

In gold there is further evidence that stage III results from vacancy migration. In gold, electron irradiated at 130 °K, Shimomura[31] observes interstitial platelets by electron microscopy. In films thinned after warming to an annealing temperature, the interstitial platelets shrank and vanished during stage-III annealing. For specimens thinned before stage-III recovery, the platelets did not completely vanish. This was attributed to vacancies reaching the surface. If the platelets were emitting interstitials there should be no difference between samples annealed in bulk form or for thinned samples.

(b) In the alloys which show GP-zone formation, the zone formation after quenching appears almost identical to samples which were irradiated. The presence of the interstitial clusters does not appear to influence the zone formation.

The major experimental results found in these experiments are as follows:

(a) The production curves of dilute aluminum alloys upon irradiation at 80 °K by 2- and 3-MeV electrons are much enhanced in comparison to pure aluminum. This shows that impurities (Mg, Ag, Au, Zn, and Ge) trap interstitials.

(b) Two annealing stages normally seen below stage III are enhanced in Mg-, Ag-, Zn-, and Ge-doped aluminum. Al-Au alloys do not have annealing stages below stage III. These stages are probably due to the break up of interstitials from the impurity atoms or clusters.

(c) Below and above stage III, reverse recovery of electrical resistivity was observed in some alloys. Zn- and Ge-doped aluminum alloys showed the reverse recovery below stage III. This is due to the formation of GP zones by the migration of vacancy-impurity complexes. The reverse recovery above stage III is due to the GP-zone

---

TABLE III. Stage III activation energies.

Material	Activation energies as obtained by Primak analysis			Fig.
	Main peak "C"	B peak	A peak	
Pure Al	0.60 ± 0.02	$\cdots$	$\cdots$	14
Al–Zn	0.61 ± 0.03	$\cdots$	0.37 ± 0.03	15
Al and Mg	0.61 ± 0.04	0.54 ± 0.04	0.37 ± 0.04	
Al and Ag	0.62 ± 0.03	0.55 ± 0.03	0.38 ± 0.03	
Al and Ge	0.61 ± 0.04	0.47 ± 0.04	0.34 ± 0.04	
Al and Au	0.61 ± 0.04	$\cdots$	$\cdots$	16

formation as found in a normal recovery process.

(d) Stage III in aluminum is not affected by alloying Mg, Zn, Ge, Ag, and Au. The activation energy for the annealing is calculated to be 0.60 ± 0.03 eV, which is the same as that for pure aluminum.

This activation energy is also the same as that in a quenching experiment in aluminum. However, the temperature associated with stage III is normally lower than that of pure aluminum because of the high damage and the low number of jumps for a defect to reach a sink and the difference in sink densities.

We conclude that stage-III recovery in aluminum and aluminum alloys occurs by the migration of vacancies to interstitial clusters or to interstitials trapped by impurity atoms. Grenning and Koehler[18] also found that there was not much change in the activation energy associated with stage III in Ag, Cu, and Au dilute alloys.

ACKNOWLEDGMENT

---

[1]J. S. Koehler, in Vacancies and Interstitials in Metals, edited by A. Seeger, D. Schumacher, W. Schilling, and J. Diehl (Wiley, New York, 1970), p. 989.

[2]R. R. Hasiguti, Proc. Japan. Acad. 26, 335 (1960).

[3]R. R. Hasiguti, J. Phys. Soc. Japan 15, 1807 (1960).

[4]T. Federighi, S. Ceresara, and F. Pieragostini, Phil. Mag. 12, 1093 (1965).

[5]S. Ceresara, T. Federighi, and F. Pieragostini, Phys. Letters 6, 152 (1963).

[6]S. Ceresara, H. Elkholy, T. Federighi, and F. Pieragostini, Phys. Letters 16, 9 (1965).

[7]T. Federighi, S. Ceresara, and F. Pieragostini, Phil. Mag. 12, 1093 (1965).

[8]Y. N. Lwin, M. Doyama, and J. S. Koehler, Phys. Rev. 165, 787 (1968).

[9]A. Sosin and L. H. Rachal, Phys. Rev. 130, 2238 (1963).

[10]K. R. Garr and A. Sosin, Phys. Rev. 162, 681 (1967).

[11]P. B. Peters and P. E. Shearin, Phys. Rev. 174, 691 (1968).

[12]W. Bauer, in Vacancies and Interstitials in Metals, edited by A. Seeger, D. Schumacher, W. Schilling, and J. Diehl (Wiley, New York, 1970), p. 275.

[13]C. Frois and O. Dimitrov, Compt. Rend. 263, 1496 (1966).

[14]C. Frois and O. Dimitrov, Compt. Rend. 258, 5647 (1964).

[15]C. Frois and O. Dimitrov, in Vacancies and Interstitials in Metals, edited by A. Seeger, D. Schumacher, W. Schilling, and J. Diehl (Wiley, New York, 1970), p. 290.

[16]C. Budin and P. Lucasson, Phys. Letters 16, 229 (1965).

[17]F. Dworschak, K. Herschbach, and J. S. Koehler, Phys. Rev. 133, A293 (1963).

[18]D. A. Grenning and J. S. Koehler, Phys. Rev. 144, 4396 (1966).

[19]G. J. Dienes and A. C. Damask, Point Defects in Metals (Gordon and Breach, New York, 1963), p. 147.

[20]T. Federighi, in Lattice Defects in Quenched Metals, edited by R. M. J. Cotterill, M. Doyama, J. J. Jackson, and M. Meshii (Academic, New York, 1965), p. 217.

[21]Hansen, Constitution of Binary Alloys (McGraw-Hill, New York, 1958).

[22]See R. Berliner and C. C. Lee, in A. Gordon, Ph.D. thesis, University of Illinois, Urbana, Illinois, 1969 (unpublished).

[23]C. Lee and J. S. Koehler, Phys. Rev. 176, 813 (1968).

[24]W. Primak, Phys. Rev. 100, 1677 (1955); J. Appl. Phys. 31, 1524 (1960).

[25]G. D. Magnuson, W. Palmer, and J. S. Koehler, Phys. Rev. 109, 1990 (1958).

[26]J. H. Bredt, Ph.D. thesis, University of Illinois, Urbana, Illinois, 1960 (unpublished).

[27]K. Herschbach, Phys. Rev. 130, 554 (1963).

[28]W. Bauer, J. DeFord, J. S. Koehler, and J. W. Kauffman, Phys. Rev. 128, 1497 (1962).

[29]A. N. Lowman, N. Davis, and A. Levenson, Bull.

Am. Math. Soc. 48, 739 (1942).

[30]N. L. Peterson and S. J. Rothman (private commun-

ication).

[31]Y. Shimomura, Phil. Mag. 19, 773 (1969).

Magnetoacoustic Absorption of Longitudinal Sound
in Magnesium in High Magnetic Fields[†][*]

Robert W. Reed and F. G. Brickwedde

Department of Physics, The Pennsylvania State University, University Park, Pennsylvania 16802

(Received 10 June 1970)

Pulse-echo measurements were made of the oscillations in the attenuation of 100–420 MHz longitudinal sound in single crystals of Mg [99.95%; $R(300 \text{ K})/R(4.2 \text{ K}) \sim 425$]. The $\vec{q}$ in different specimens was parallel to the [0001], [11$\bar{2}$0], and [10$\bar{1}$0] axes; H was varied from 1 to 40 kOe. The temperature was varied from 1 to 4.2 K, and ql from 0.4 to 1.8. Areas of extremal-sized cross sections of the Fermi surface, oriented perpendicular to $\vec{H}$, were calculated from the $\Delta(1/H)$ periods in attenuation. These areas are in good agreement with Stark's values from de Haas–van Alphen–effect data using much purer Mg, with the exception of the μ_1^5 area, where there is a 2% difference. The short $\Delta(1/H)$-period magnetoacoustic oscillations corresponding to the large-area λ_1^1 oscillations were modulated with the long period corresponding to the small μ_1^5 area, and the λ_2^1 oscillation was modulated with the period corresponding to the μ_2^1 area. This phenomenon is not satisfactorily explained. A simple derivation is given for magnetoacoustic oscillations (periods and amplitudes) on the assumption that the only effect of $\vec{H}$ on the attenuation is through its effect on the density of states at the Fermi surface. The de Haas–van Alphen ($ql < 0.7$) and intermediate ($ql > 0.7$) regions of magnetoacoustic absorption are included. The dependence of the oscillation amplitudes on H, T, τ, ql, and the direction of $\vec{q}$ was checked experimentally.

I. INTRODUCTION

This is a report on the investigation of the oscillations in the magnetoacoustic (MA) absorption of longitudinal sound in single crystals of Mg as $\vec{H}$ was varied in magnitude and direction. The investigation was carried out with 100–420 MHz sound, at temperatures between 1.0 and 4.2 K, in fields from 1 to 40 kOe, using single crystals[1] of Mg having resistance ratios between 350 and 450. The product ql (q is the sonic wave number $2\pi/\lambda$, and l is the electron mean free path) in our investigation was of order 1. This puts our investigation in a region of ql in which the oscillations in the ultrasonic attenuation coefficient $\alpha(B)$ have an origin similar to the origin of the oscillations of the magnetic susceptibility in the de Haas–van Alpen (dHvA) effect. As a consequence, the MA oscillations we observed were similar in frequency, temperature and field dependence of amplitude, and line shape to the oscillations in the dHvA effect.

The MA oscillations in $\alpha(B)$ are periodic in $1/B$. The $1/B$ periods are proportional to reciprocals of extremal values of the cross-sectional areas of the Fermi surface (FS) in k space sectioned by planes perpendicular to $\vec{B}$. The areas are extremal with respect to displacements of the intersecting plane along the axis of $\vec{B}$. The FS is oriented with respect

to the crystal axes; by varying the orientation of the axes of a crystal with respect to the solenoid field $\vec{H}$, extremal areas for all orientations relative to the crystal axes are, in principle, obtainable. The extremal areas, in conjunction with theoretically determined electron band structures and electron constant-energy surfaces in $\vec{k}$ space, make possible determinations of the actual shape and size of the FS, and with this information to calculate a *pseudopotential* for the conduction electrons.[2]

The FS of Mg has been investigated experimentally by others and by other methods.[3–7] The most recent and complete measurements on Mg are the MA measurements of the geometric-resonance type ($ql \gg 1$) by Ketterson and Stark,[8] and the dHvA-effect measurements by Stark.[9] Our MA data (extremal cross sections of the FS) are compared with accurate data by Stark[9] from dHvA measurements. The labeling of cross sections of the FS in our paper was adopted from Stark.[9]

A theory for MA oscillations is presented for the region $\omega\tau \ll 1$ (ω is the sonic angular frequency, τ is the relaxation time for an electron). The ideas and mathematics are not original, but as far as we are aware, the theory for MA absorption in the $\omega\tau \ll 1$ region has not been presented before in the mathematically simple method followed here.

We investigated experimentally the dependence of